

Available online at www.sciencedirect.com

ScienceDirect

Physics Procedia 61 (2015) 828 – 837

Physics

Procedia

Limit on neutrinoless double beta decay of ^{76}Ge by GERDA

M. Agostiniⁿ, M. Allardt^c, E. Andreotti^q, A.M. Bakalyarov^l, M. Balata^a, I. Barabanov^j, M. Barabè Heider^{f,n}, N. Barros^c, L. Baudis^r, C. Bauer^f, N. Becerici-Schmidt^m, E. Bellotti^{g,h}, S. Belogurov^{k,j}, S.T. Belyaev^l, G. Benato^r, A. Bettini^{o,p}, L. Bezrukov^j, T. Bodeⁿ, V. Brudanin^d, R. Brugnera^{o,p}, D. Budjásⁿ, A. Caldwell^m, C. Cattadori^h, A. Chernogorov^k, F. Cossavella^m, E.V. Demidova^k, A. Domula^c, V. Egorov^d, R. Falkenstein^q, A. Ferella^r, K. Freund^q, N. Frodyma^b, A. Gangapshev^{j,f}, A. Garfagnini^{o,p}, C. Gotti^{g,h}, P. Grabmayr^d, V. Gurentsov^j, K. Gusev^{l,d,n}, K.K. Guthikonda^f, W. Hampel^f, A. Hegai^q, M. Heisel^f, S. Hemmer^{o,p}, G. Heusser^f, W. Hofmann^f, M. Hult^c, L.V. Inzhchik^j, J. Janicskó Csáthyⁿ, J. Jochum^q, M. Junker^a, T. Kihm^f, I.V. Kirpichnikov^k, A. Kirsch^f, A. Klimenko^{f,d}, K.T. Knöpfle^f, O. Kochetov^d, V.N. Kornoukhov^{k,j}, V.V. Kuzminov^j, M. Laubenstein^a, A. Lazzaroⁿ, V.I. Lebedev^l, B. Lehnert^c, H.Y. Liao^m, M. Lindner^f, I. Lippi^p, A. Lubashevskiy^f, B. Lubsandorzhev^j, G. Lutter^e, A.A. Machado^f, C. Macolino^a, B. Majorovits^m, W. Maneschg^f, M. Misiaszek^b, I. Nemchenok^d, S. Nisi^a, C.O' Shaughnessy^m, L. Pandola^a, K. Pelczar^b, G. Pessina^{g,h}, A. Pulliaⁱ, S. Riboldiⁱ, N. Rumyantseva^d, C. Sada^{o,p}, M. Salathe^f, C. Schmitt^q, J. Schreiner^f, O. Schulz^m, B. Schwingenheuer^f, S. Schönertⁿ, E. Shevchik^d, M. Shirchenko^{l,d}, H. Simgen^f, A. Smolnikov^f, L. Stanco^p, H. Strecker^f, M. Tarka^r, C.A. Ur^p, A.A. Vasenko^k, O. Volynets^m, K. von Sturm^{o,p}, V. Wagner^f, M. Walter^r, A. Wegmann^f, T. Wester^c, M. Wojcik^b, E. Yanovich^j, P. Zavarise^a, I. Zhitnikov^d, S.V. Zhukov^l, D. Zinatulina^d, K. Zuber^c, G. Zuzel^b

^a INFN Laboratori Nazionali del Gran Sasso, LNGS, Assergi, Italy^b Institute of Physics, Jagiellonian University, Cracow, Poland^c Institut für Kern- und Teilchenphysik, Technische Universität Dresden, Dresden, Germany^d Joint Institute for Nuclear Research, Dubna, Russia^e Institute for Reference Materials and Measurements, Geel, Belgium^f Max-Planck-Institut für Kernphysik, Heidelberg, Germany^g Dipartimento di Fisica, Università Milano Bicocca, Milano, Italy^h INFN Milano Bicocca, Milano, Italyⁱ Dipartimento di Fisica, Università degli Studi di Milano e INFN Milano, Milano, Italy^j Institute for Nuclear Research of the Russian Academy of Sciences, Moscow, Russia^k Institute for Theoretical and Experimental Physics, Moscow, Russia^l National Research Centre "Kurchatov Institute", Moscow, Russia^m Max-Planck-Institut für Physik, München, Germanyⁿ Physik Department and Excellence Cluster Universe, Technische Universität München, Germany^o Dipartimento di Fisica e Astronomia dell'Università di Padova, Padova, Italy^p INFN Padova, Padova, Italy^q Physikalisches Institut, Eberhard Karls Universität Tübingen, Tübingen, Germany^r Physik Institut der Universität Zürich, Zürich, Switzerland**Abstract**

The GERDA experiment at the Laboratori Nazionali del Gran Sasso in Italy uses germanium detectors made from material with an enriched ^{76}Ge isotope fraction to search for neutrinoless double beta decay of this nucleus. Applying a blind analysis we find no signal after an exposure of 21.6 kg·yr and a background of about 0.01 cts/(keV·kg·yr). A half-life limit of $T_{1/2}^{0\nu} > 2.1 \cdot 10^{25}$ yr (90% C.L.) is extracted. The previous claim of a signal for ^{76}Ge is excluded with 99% probability in a model independent way.

© 2015 The Authors. Published by Elsevier B.V. This is an open access article under the CC BY-NC-ND license (<http://creativecommons.org/licenses/by-nc-nd/4.0/>).

Selection and peer review is the responsibility of the Conference lead organizers, Frank Avignone, University of South Carolina, and Wick Haxton, University of California, Berkeley, and Lawrence Berkeley Laboratory

Keywords: double beta decay



Fig. 1. Model of the GERDA experiment. The labels are: 1 = detector array (not to scale), 2 = cryostat, 3 = inner copper lining, 4 = water tank, 5 = clean room, 6 = lock for Ge detector insertion.

1. Introduction

Lepton number is not conserved in neutrinoless double beta ($0\nu\beta\beta$) decay of isotopes like ^{76}Ge . This process is predicted to occur by many extensions of the standard model [1, 2, 3, 4]. Consequently, there is large interest to search for this process and a number of experimental programs using different experimental techniques and isotopes are currently taking data or will soon start [5, 6].

The GERDA experiment located at the Laboratori Nazionali del Gran Sasso (LNGS) of INFN in Italy operates germanium diodes as detectors and sources of $0\nu\beta\beta$ decay of ^{76}Ge . The ^{76}Ge isotope fraction of the detector material is enriched from 7.8 % to ≈ 86 %. The signature of the decay is a peak at $Q_{\beta\beta} = 2039.061 \pm 0.007$ keV [7] in the measured energy spectrum.

Part of the Heidelberg-Moscow collaboration has claimed to have observed 28.75 ± 6.86 $0\nu\beta\beta$ decay events of ^{76}Ge [8]. This observation converts to a half-life of $T_{1/2}^{0\nu} = (1.19_{-0.23}^{+0.37}) \cdot 10^{25}$ yr. Later, the pulse shapes of the detector signals have been analyzed to strengthen the significance of the observation [9]. We restrict our comparison to the first publication since there are some problems in the later publication like the missing efficiency correction in the derived half-life [10].

Recently, Kamland-Zen [11] and EXO-200 [12] have report 90 % C.L. half-life limits for $0\nu\beta\beta$ decay of ^{136}Xe of $1.9 \cdot 10^{25}$ yr and $1.6 \cdot 10^{25}$ yr, respectively. Nuclear matrix element calculations are needed to relate these results to the claim for ^{76}Ge which complicates the comparison. This is not the case for GERDA since we use the same isotope. We report here about our first result which is published in [13].

2. Experiment and data selection

GERDA operates refurbished semi-coaxial diodes from the Heidelberg-Moscow experiment [14] and from the International GERmanium eXperiment (IGEX) [15, 16]. Here we report results from the first measurement period from November 2011 to May 2013. Five newly produced detectors of BEGe type [17] have been added in July 2012. In addition, we operated one semi-coaxial detector with natural isotope composition. Two semi-coax detectors exhibited a large leakage current soon after the deployment and were not used. The leakage current of all other detectors was stable within 20 pA. One BEGe showed unstable energy

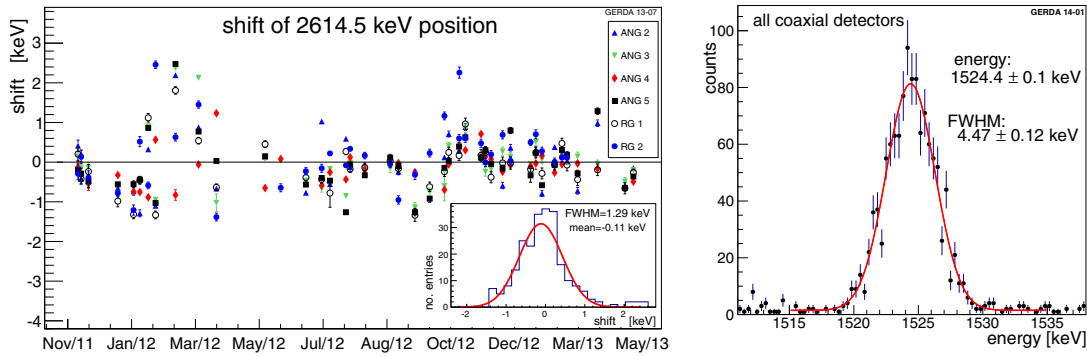


Fig. 2. Left: Shift of the 2615 keV calibration peak position between consecutive calibrations for the individual semi-coaxial detectors. The detector names are listed in the legend. The insert shows the projection of the shifts. Right: ^{42}K peak in physics data of all semi-coaxial detectors.

calibration and was therefore also not included in the analysis. A detailed description of the experiment is given in Ref. [18].

The detectors are mounted in low mass copper holders and operated in 64 m^3 liquid argon which serves as coolant and as shield against external background radiation. The shielding is complemented by 3 m of water which is instrumented with photo multipliers to detect the Cerenkov light of muons traversing the setup. Fig. 1 shows a model of GERDA.

Each detector signal is read out by a charge sensitive amplifier located at close distance of ≈ 30 cm to the detectors in the liquid argon. The outputs are digitized with 100 MHz Flash ADCs. All event parameters like the deposited energy or the rise time of the detector signal are reconstructed by digital filters offline [19, 20]. Unphysical events triggered e.g. by noise are identified and rejected. A visual scan of all events with energy deposition between 1.3 and 2.7 MeV showed that no real event was rejected and that no unphysical event is kept.

The energy reconstruction and noise rejection was cross checked with a second completely independent algorithm. The selected event samples around $Q_{\beta\beta}$ were identical and the reconstructed energies agreed with each other within $\sigma = 0.9$ keV.

$0\nu\beta\beta$ decays deposit almost always energy in only one detector. Events with depositions in several detectors or in correlation with a muon candidate (within $8\ \mu\text{s}$) are therefore not considered. These requirements remove about 40 % of the events around $Q_{\beta\beta}$. Two events within 1 ms in the same detector are most likely from the ^{214}Bi - ^{214}Po decay chain and therefore rejected. These cuts cause practically no dead time.

To calibrate the energy, we collect (bi)weekly data sets with ^{228}Th sources deployed close to the detectors. Fig. 2 (left) shows for the semi-coaxial detectors the drift of the 2615 keV peak relative to the position of the corresponding previous calibration. The gain drifts by typically less than 0.05 % which is small relative to the typical energy resolution of 0.2 % at $Q_{\beta\beta}$ (full width at half maximum, FWHM). Fig. 2 (right) shows the strongest background peak of the physics data from ^{42}K decays. The reconstructed peak position agrees within 0.3 keV with the nominal value of 1524.7 keV which is also true for weaker lines in the spectrum. The fitted resolution (FWHM) of 4.5 keV is only slightly larger than the value of 4.3 keV expected from calibration data. From this comparison and the known extrapolation of the resolution to $Q_{\beta\beta}$ we expect for the semi-coaxial detector an average resolution of 4.8 ± 0.3 keV and 3.2 ± 0.2 keV for the BEGe detectors. The resolution of all detectors was stable within 0.1 keV during the entire data taking period. All numbers show that the detector performance was sufficiently stable and that the physics data is well calibrated.

We performed a blind analysis. Events in the interval $Q_{\beta\beta} \pm 20$ keV were hidden until the calibration was finalized and all selection cuts were frozen.

Visible γ peaks in the energy spectrum (see Fig. 3) are from ^{40}K and ^{42}K decays and the decay chains of ^{226}Ra and ^{232}Th . Between the trigger threshold of 40-100 keV and 570 keV, the spectrum is dominated

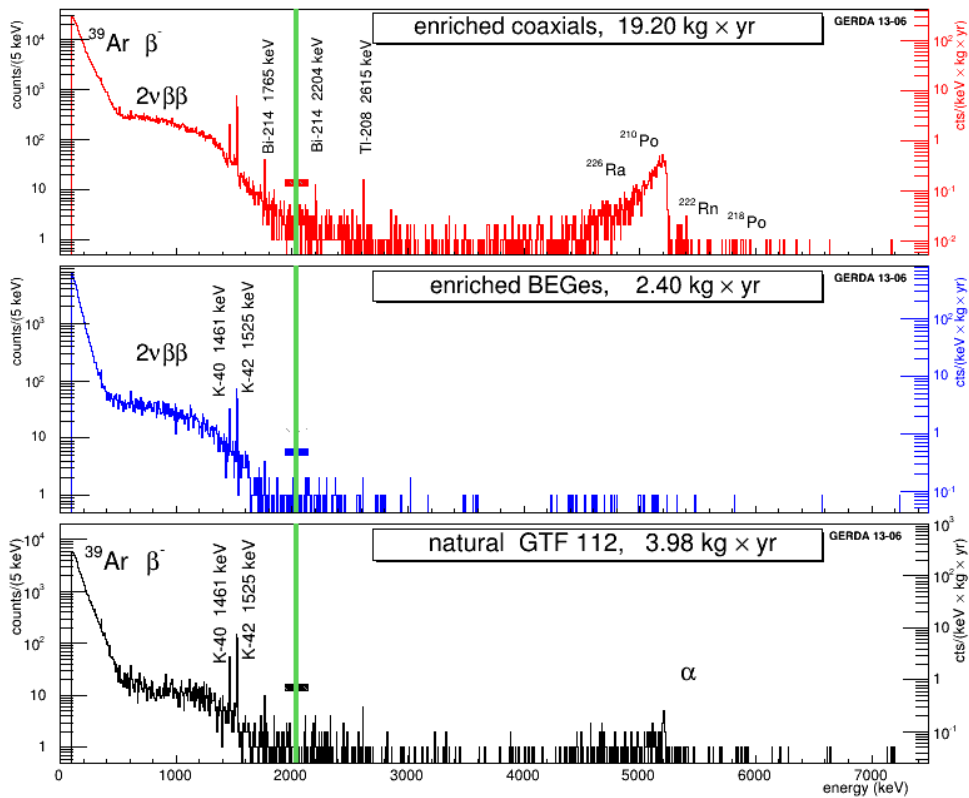


Fig. 3. Spectra of physics data for semi-coaxial, BEGe and natural detectors [22].

by ^{39}Ar β decays; between 570 keV and 1700 keV the main contribution is from double beta decay with neutrino emission ($2\nu\beta\beta$ decays) [21]. Above 3 MeV we observe α decays on the detector p^+ contact surfaces; predominantly from ^{210}Po but to a smaller extent also from the ^{226}Ra decay chain. Around 2 MeV, we observe a mixture of contributions [22].

We fit the physics spectrum of the semi-coaxial and the BEGe detectors between 570 and 7500 keV to a background model consisting of the above mentioned contributions at different locations. Despite the fact that the location and composition of the events around $Q_{\beta\beta}$ can not be determined precisely with the available statistics (see Fig. 4), we know that the background

- is largely dominated by sources close to the detectors or on the detector surfaces,
- is not expected to have a peak in the blinded energy window,
- can be well approximated by a constant intensity in the energy window from 1930 - 2190 keV with the exclusion of two intervals at 2104 ± 5 keV and 2119 ± 5 keV where we expect sizable contributions from known γ peaks. Other lines expected in this window from e.g. ^{214}Bi decays are too weak ($\ll 1$ count) to be relevant.

If bremsstrahlung energy loss of electrons in $0\nu\beta\beta$ events is small, all ionization occurs in a small volume of the detector (single site events). Background events from Compton scattered photons deposit often energy in several well separated locations (multi site events). The induced current signal on the readout electrode will in general be different for the two classes. Surface background events also exhibit distinct signal shapes. This feature is used in GERDA to discriminate background events. A detailed description of the algorithms is given in Ref. [23]. Here, we will only discuss them briefly.

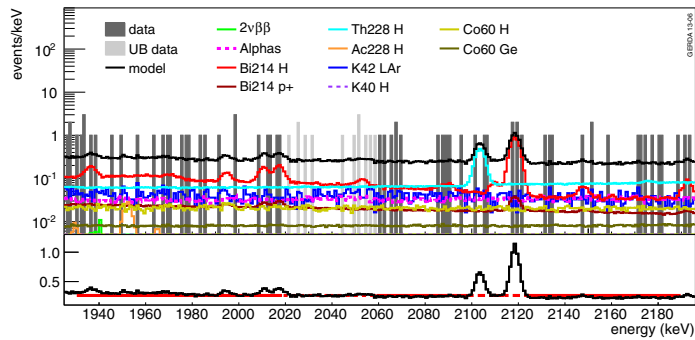


Fig. 4. Spectrum of physics data for the semi-coaxial enriched detectors around $Q_{\beta\beta}$ and the composition according to a fit with different possible contributions on a logarithmic scale. The bottom plot shows the model and a flat background on a linear scale. The labels for the location mean “p+” on p^+ detector surface, “H” close to the detector, e.g. in the holder, “LAr” homogeneous in the argon, “Ge” inside the Ge detectors [22]. The interval $Q_{\beta\beta} \pm 20$ keV was blinded and not used for the fit. The light grey part of the histogram shows the partially unblinded interval.

For BEGe detectors, the ratio of the maximum of the current pulse, A , over the deposited energy, E , allows for a simple, powerful and robust selection. Double escape peak (DEP) events of 2615 keV photons from ^{208}Tl decays of the calibration data serve as proxy for the pulse shape of $0\nu\beta\beta$ decays. For the accepted range of $0.965 < A/E < 1.07$ we find a signal efficiency of 0.92 ± 0.02 while more than 80 % of the background events around $Q_{\beta\beta}$ are removed. We cross check the signal efficiency with $2\nu\beta\beta$ decays in the interval 1.0 - 1.4 MeV. The value of 0.91 ± 0.05 agrees well.

For the semi-coaxial detectors, the neural network algorithm TMlpANN implemented in TMVA [24] is used to identify single site events. The times when the charge pulses reach 1%, 3%, ..., 99% of the maximum are the input variables. Two hidden layers with 51 and 50 neurons are used. For training, DEP events at 1593 keV serve as signal sample and gamma events at 1621 keV from ^{212}Bi decays serve as multi site event sample. The training is performed for each detector and for three periods of similar conditions. The cut on the classifier output of the neural network is chosen to retain 90 % of the DEP.

To cross check the selection, two independent algorithms based on a projective likelihood method implemented in TMVA and on the current pulse asymmetry have been developed. Of the physics data events between 1930 and 2190 keV (outside the blinded window) about 45 % are rejected by the neural network. All of these events are rejected by at least one other method and about 90 % of them are rejected by both. This gives confidence that the classification of background events by the neural network is meaningful.

We assume that the pulse shape selection efficiency for $0\nu\beta\beta$ decays is the same as for the DEP events used for training. To cross check this assumption, the efficiency for $2\nu\beta\beta$ events in the energy interval 1.0 - 1.3 MeV was measured to be 0.85 ± 0.02 for the total data set. A special calibration data set with a ^{56}Co source was taken since this spectrum has two usable DEPs at 1576 keV and at 2231 keV, see Fig. 5. Applying the neural network selection we find for the different detectors efficiencies between 83 % and 95 % for the two additional DEPs. In summary, we estimate the efficiency and the systematic uncertainty of the $0\nu\beta\beta$ selection to be $0.90^{+0.05}_{-0.09}$.

Our pulse shape selections are intended to yield the best sensitivity for a $T_{1/2}^{0\nu}$ limit: The expected background counts at $Q_{\beta\beta}$ are low and hence only a moderate rejection is needed while keeping the efficiency high. It is worth to notice that all DEPs reconstruct at the correct energy, independent whether the pulse shape selection is applied or not. Hence we expect that a possible $0\nu\beta\beta$ decay signal reconstructs at $Q_{\beta\beta}$.

3. Results

The data are split into three sets. One contains the BEGe data. A second one (labelled “silver” set) covers a short period of semi-coaxial data with higher background index at the time when the BEGe detectors were

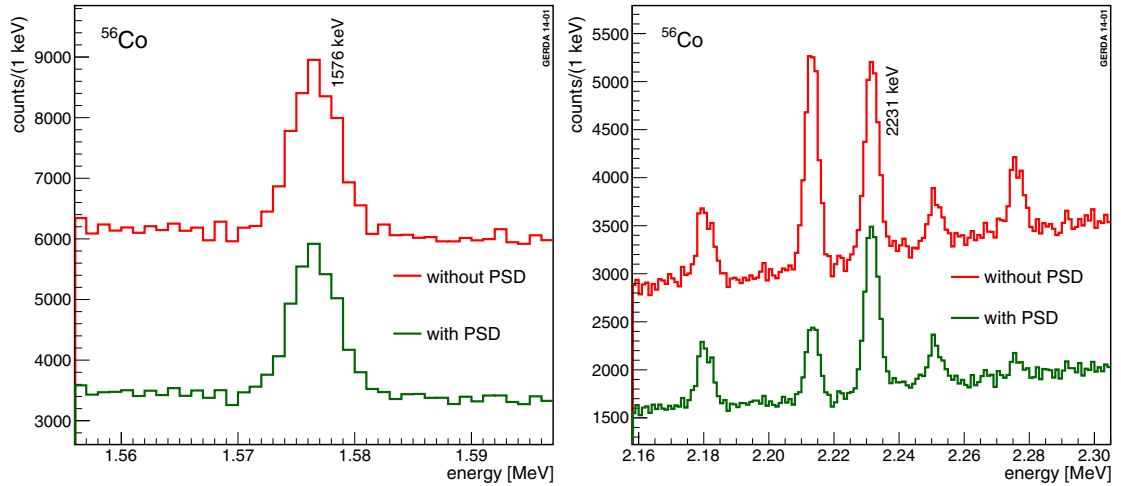


Fig. 5. Part of the ^{56}Co calibration spectrum without (red) and with (green) pulse shape selection. The main DEPs are at 1576 keV (left) and at 2231 keV (right). At 2180 keV and 2251 keV are DEPs with lower statistics.

deployed. The rest of the semi-coaxial data is labelled “golden” set. The relevant analysis parameters of all sets are listed in Tab. 1.

After the analysis methods discussed above have been frozen, the events in the blinded window have been processed. The expected background counts and observed number of events are consistent in all sets, with and without pulse shape discrimination (see last two columns of Tab. 1 and Fig. 6). Hence, GERDA sees no indication for a $0\nu\beta\beta$ decay signal and a half-life limit is extracted. All results are given with pulse shape discrimination applied.

The observed signal count $N_k^{0\nu}$ (or limit) for each data set $k = (\text{golden, silver, BEGe})$ is related to the half-life $T_{1/2}^{0\nu}$ by

$$N_k^{0\nu} = \frac{\ln 2 \cdot N_A \cdot \epsilon_k \cdot \mathcal{E}_k}{m_A \cdot T_{1/2}^{0\nu}} \quad (1)$$

where N_A is Avogadro’s constant, ϵ_k is the efficiency, \mathcal{E}_k the exposure and $m_A = 0.0756$ kg the molar mass of the enriched material. ϵ_k is the product of the (set dependent) enrichment fraction f_{76} , the active volume fraction of the detectors f_{av} , the fraction of $0\nu\beta\beta$ events which deposit all energy in the active volume f_{dep} and the pulse shape selection efficiency discussed above.

We fit each of the energy spectra of the three sets to a normalized function $f(E | b_k, 1/T_{1/2}^{0\nu})$ which is the sum of a constant b_k for the background and a Gaussian for a possible $0\nu\beta\beta$ signal. The latter is centered at $Q_{\beta\beta} \pm 0.2$ keV and has a width $\sigma_k = \delta E_k / 2.35$ (Tab. 1) given by the known energy resolution. The 240 keV wide window for the background estimate spans from 1930 keV to 2190 keV without the intervals (2104 ± 5) keV and (2119 ± 5) keV from known γ lines.

$$f(E | b_k, 1/T_{1/2}^{0\nu}) = \frac{1}{240 \text{ keV} \cdot b_k + N_k^{0\nu}} \left(b_k + \frac{N_k^{0\nu} (1/T_{1/2}^{0\nu})}{\sqrt{2\pi} \cdot \sigma_k} \exp\left(-\frac{(E - Q_{\beta\beta})^2}{2\sigma_k^2}\right) \right) \quad (2)$$

with $N_k^{0\nu} (1/T_{1/2}^{0\nu})$ given by Eq. 1.

We perform a profile likelihood fit. The (unbinned extended) likelihood L is

$$L(b_k, 1/T_{1/2}^{0\nu}) = \prod_k \frac{\mu_k^{N_k} \cdot e^{-\mu_k}}{N_k!} \prod_{\text{events}} f(E | b_k, 1/T_{1/2}^{0\nu}) \quad (3)$$

with N_k being the number of observed events in data set k and $\mu_k = b_k \cdot 240 \text{ keV} + N_k^{0\nu}$ the expected number

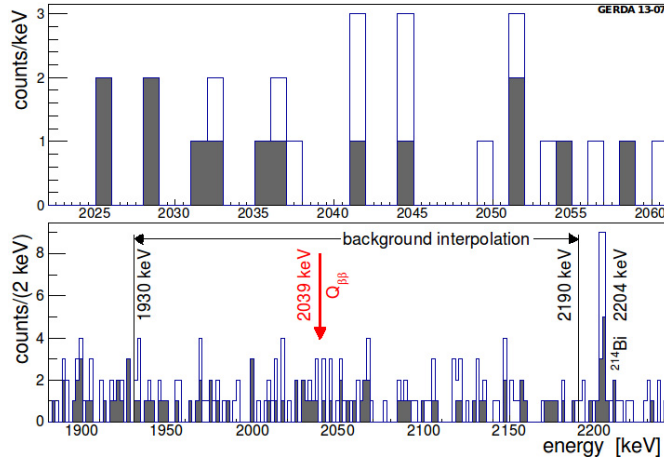


Fig. 6. Physics spectrum of all 3 data sets after unblinding without (histogram) and with (solid grey) pulse shape selection [13].

Table 1. List of analysis parameters for the three sets without and with pulse shape discrimination. ϵ_k is the total $0\nu\beta\beta$ decay detection efficiency. δE_k is the energy resolution (FWHM). The total detector mass is used to calculate the “exposure” \mathcal{E}_k . “bkg” is the number of events in the 1930-2190 keV window (without the intervals (2039 ± 5) keV, (2114 ± 5) keV and (2119 ± 5) keV) and “BI” is the corresponding background index. “ROI exp” is the expected background count in a ± 5 keV window around $Q_{\beta\beta}$ and “ROI obs” is observed counts after the unblinding.

set k	ϵ_k	δE_k keV	exposure kg·yr	bkg	BI $10^{-3}\text{cts}/(\text{keV}\cdot\text{kg}\cdot\text{yr})$	ROI exp	ROI obs
without PSD							
golden	0.688 ± 0.031	4.8	17.9	76	18 ± 2	3.3	5
silver	0.688 ± 0.031	4.6	1.3	19	63^{+16}_{-14}	0.8	1
BEGe	0.720 ± 0.018	3.2	2.4	23	42^{+10}_{-8}	1.0	1
with PSD							
golden	$0.619^{+0.044}_{-0.070}$	4.8	17.9	45	11 ± 2	2.0	2
silver	$0.619^{+0.044}_{-0.070}$	4.6	1.3	9	30^{+11}_{-9}	0.4	1
BEGe	0.663 ± 0.022	3.2	2.4	3	5^{+4}_{-3}	0.1	0

of events. The product for L is over all events in all data sets. The profile likelihood $\lambda(1/T_{1/2}^{0\nu})$ is then

$$\lambda(1/T_{1/2}^{0\nu}) = \frac{\max_{b_k} L(b_k, 1/T_{1/2}^{0\nu})}{\max_{\hat{b}_k, 1/\hat{T}_{1/2}^{0\nu}} L(\hat{b}_k, 1/\hat{T}_{1/2}^{0\nu})} \quad (4)$$

In the fit we require $1/T_{1/2}^{0\nu} \geq 0$, i.e. $N_k^{0\nu} \geq 0$. The 90 % coverage limit is defined as the $1/T_{1/2}^{0\nu}$ value for which $-2 \cdot \ln \lambda$ changes by 2.7. We verified with a toy Monte Carlo that the coverage of this method is sufficient. The best fit yields $1/T_{1/2}^{0\nu} = 0$ and the limit is

$$T_{1/2}^{0\nu} > 2.1 \cdot 10^{25} \text{ yr (90 \% C.L.)} \quad (5)$$

Systematic uncertainties on the peak position, the resolution, and all efficiencies are taken into account by a Monte Carlo method: the half-life limit is calculated for 10000 randomly chosen parameter sets according to the known distributions. The quoted limit is the average over all individual limits. Without the systematic uncertainties the limit improves by 1.5 %. The (median) sensitivity is $2.4 \cdot 10^{25}$ yr.

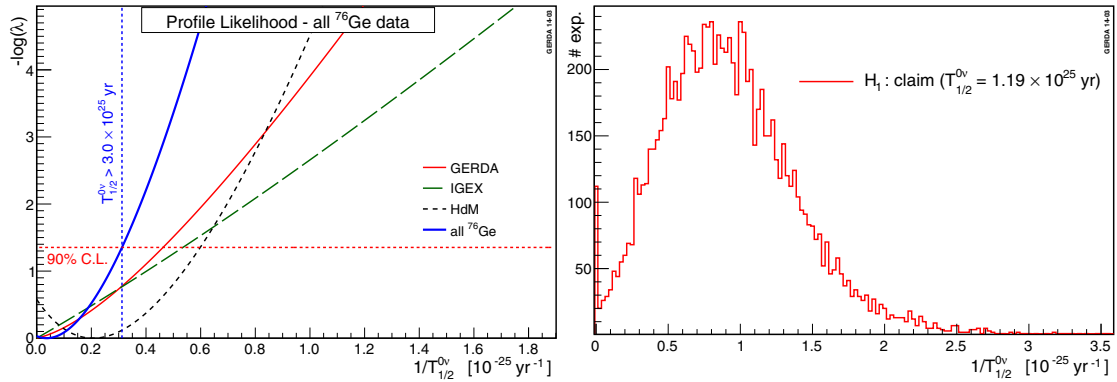


Fig. 7. Left: Profile likelihood distribution for the individual Ge experiments and the combination. Right: Best fitted $1/T_{1/2}^{0\nu}$ for 10000 toy Monte Carlo realizations of the experiment for the hypothesis H_1 of a signal according to the claim. The bin size is $0.025 \cdot 10^{-25} \text{ yr}^{-1}$.

We perform also a Bayesian analysis. A binned likelihood fit and the above mentioned sampling method for the systematic error are used. The fit is performed with the BAT toolkit [25] and a flat prior in $1/T_{1/2}^{0\nu}$ between 0 and 10^{-24} yr^{-1} . The posterior distribution peaks at $1/T_{1/2}^{0\nu} = 0$ and the 90 % credible limit is $T_{1/2}^{0\nu} > 1.9 \cdot 10^{25} \text{ yr}$. The (median) sensitivity is $2.0 \cdot 10^{25} \text{ yr}$.

The spectral fit can be extended to include the spectra from Heidelberg-Moscow (interval 2000-2080 keV, Fig. 4 of Ref. [14]) and IGEX (interval 2020-2060 keV, Table II of Ref. [15]). We assume that the backgrounds are constant as a function of energy in these intervals. Experimental parameters (exposure, energy resolution, efficiency factors) are obtained from the original references or, when not available, extrapolated from the values used in GERDA. Fig. 7 (left) shows the profile likelihood curves for the individual experiments and the combination. The latter yields

$$T_{1/2}^{0\nu} > 3.0 \cdot 10^{25} \text{ yr} \quad (90 \% \text{ C.L.}). \quad (6)$$

4. Comparison to other experiments

We perform a hypothesis test using the $0\nu\beta\beta$ half-life of the claimed signal [8] (hypothesis H_1). In this case we would expect 5.9 ± 1.4 signal events in the energy interval of $Q_{\beta\beta} \pm 2\sigma_k$ above a background of 2.0 ± 0.3 counts. In a frequentist analysis we generate 10000 toy experimental spectra for each of the three data sets with Poisson distributed background and signal strength. Fig. 7 (right) shows for each realization the best fitted inverse half-life $1/T_{1/2}^{0\nu}$ from the profile likelihood fit. Only 1 % of the realizations yield our experimental result $1/T_{1/2}^{0\nu} = 0$. In case the restriction $1/T_{1/2}^{0\nu} \geq 0$ is dropped in the fit, only 0.6 % of the realizations yield $\sum_k N_k \leq 0$. Thus we reject the claim with 99 % probability.

In a Bayesian analysis we calculate the Bayes factor, i.e. the probability ratio $p(\text{data}|H_1)/p(\text{data}|H_0)$ with H_0 being the background only hypothesis. The Bayes factor is 0.024. It includes all uncertainties and clearly favors the background-only hypothesis.

Our limit can be compared to the recent results for the isotope ^{136}Xe . Neither EXO-200 nor Kamland-Zen observe a signal and they place 90 % confidence level limits of $1.6 \cdot 10^{25} \text{ yr}$ [12] and $1.9 \cdot 10^{25} \text{ yr}$ [11] for the half-life, respectively. The sensitivities are $1.0 \cdot 10^{25} \text{ yr}$ for Kamland-Zen [11] and $0.7 \cdot 10^{25} \text{ yr}$ for EXO-200 [26].¹ Fig. 8 shows the experimental limits together with a selection of different nuclear matrix element calculations for the case of light neutrino exchange.

For the sensitivity estimate, the product of the background index and the energy resolution divided by the signal detection efficiency enters. This quantity is for GERDA $0.006 \text{ cts}/(\text{mol}\cdot\text{yr}\cdot\delta E)$ (normalized to mole

¹At the time of writing EXO announced an updated result [27] based on a 3.8-fold exposure. The sensitivity is $1.9 \cdot 10^{25} \text{ yr}$ (90 % C.L.) however the limit is only $T_{1/2}^{0\nu} > 1.1 \cdot 10^{25} \text{ yr}$ (90 % C.L.). We restrict our discussion to the published value.

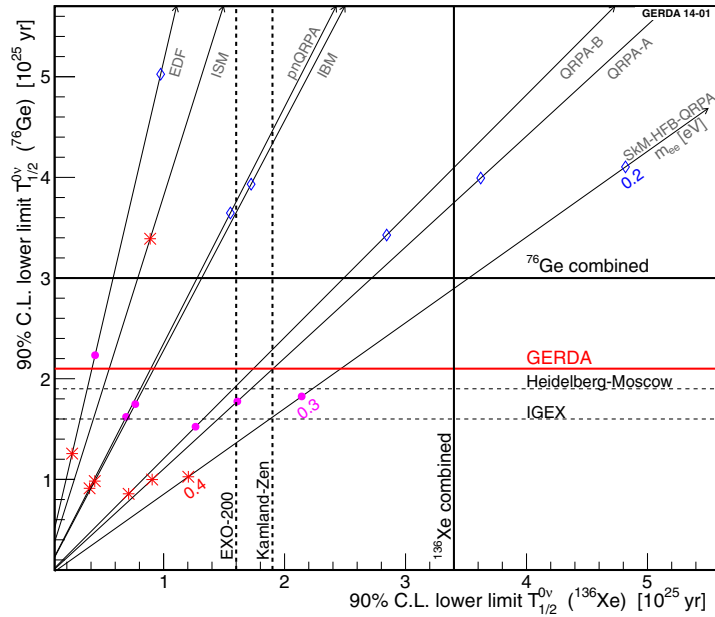


Fig. 8. Comparison of recent $T_{1/2}^{0\nu}$ limits for ^{76}Ge and ^{136}Xe and correlations of the two half-lives for different matrix element calculations (assuming light neutrino exchange). The calculations are from Ref. [28] (EDF), [29] (ISM), [30] (IBM), [31] (pnQRPA), [32] (QRPA) and [33] (SkM-HFB-QRPA). No axial vector quenching is assumed, i.e. $g_A = 1.25$. m_{ee} denotes the effective neutrino mass and values of 0.2 eV (diamonds), 0.3 eV (dots) and 0.4 eV (stars) are marked on all axes.

instead of kg), for EXO-200 about 0.044 cts/(mol·yr· δE) and for Kamland-Zen about 0.19 cts/(mol·yr· δE). This comparison explains why despite our lower exposure, GERDA reaches a half-life sensitivity which is a factor of 2 better compared to the published EXO-200 and Kamland-Zen values. However, for the calculation of physics parameters like the effective neutrino mass, also phase space factors and nuclear matrix elements enter which favor ^{136}Xe (see Fig. 8). Note, that quenching of the axial vector coupling could change the conversion strongly and heavier nuclei are typically more affected [30].

5. Summary

GERDA collected in a first phase of data taking 21.6 kg·yr of exposure with a background of about 0.01 cts/(keV·kg·yr) (after pulse shape discrimination). We performed a blind analysis and found no signal of $0\nu\beta\beta$ decay. Hence we place a limit of $T_{1/2}^{0\nu} > 2.1 \cdot 10^{25}$ yr for ^{76}Ge at 90 % C.L. The claimed $0\nu\beta\beta$ signal is ruled out with 99 % probability in a model independent way.

In a second phase, the experiment aims to improve the background to a level of 0.001 cts/(keV·kg·yr).

References

- [1] S. M. Bilenky, C. Giunti, Neutrinoless double-beta decay: A brief review, *Mod. Phys. Lett. A* 27 (2012) 1230015.
- [2] J. D. Vergados, H. Ejiri, F. Simkovic, Theory of neutrinoless double beta decay, *Rept. Prog. Phys.* 75 (2012) 106301.
- [3] W. Rodejohann, Neutrino-less double beta decay and particle physics, *Int. J. Mod. Phys. E* 20 (2011) 1833.
- [4] J. J. Gomez Cadenas, et al., The search for neutrinoless double beta decay, *Riv. Nuovo Cim.* 35 (2012) 29.
- [5] A. Piepke, Double Beta Decay: Xe experiments, these proceedings (2014).
- [6] L. Pandola, Double Beta Decay: Non-Xe experiments, these proceedings (2014).
- [7] B. J. Mount, M. Redshaw, E. G. Myers, Double-beta-decay Q values of ^{74}Se and ^{76}Ge , *Phys.Rev. C* 81 (2010) 032501. doi:10.1103/PhysRevC.81.032501.

- [8] H. V. Klapdor-Kleingrothaus, et al., Search for neutrinoless double beta decay with enriched ^{76}Ge in Gran Sasso 1990-2003, *Phys. Lett. B* 586 (2004) 198.
- [9] H. V. Klapdor-Kleingrothaus, I. Krivosheina, The evidence for the observation of neutrinoless double beta decay: the identification of neutrinoless double beta decay events from the full spectra, *Mod. Phys. Lett. A* 21 (2006) 1547.
- [10] B. Schwingenheuer, Status and prospects of searches for neutrinoless double beta decay, *Ann. Phys. (Berlin)* 525 (2013) 269.
- [11] A. Gando, et al., Limit on neutrinoless double beta decay of ^{136}Xe from the first phase of KamLAND-Zen and comparison with the positive claim in Ge-76, *Phys. Rev. Lett.* 110 (2013) 062502.
- [12] M. Auger, et al., Search for neutrinoless double-beta decay in ^{136}Xe with EXO-200, *Phys. Rev. Lett.* 109 (2012) 032505.
- [13] M. Agostini, et al., Results on neutrinoless double beta decay of ^{76}Ge from GERDA Phase I, *Phys. Rev. Lett.* 111 (2013) 122503. arXiv:1307.4720.
- [14] H. V. Klapdor-Kleingrothaus, et al., Latest results from the Heidelberg-Moscow double beta decay experiment, *Eur. Phys. J. A* 12 (2001) 147.
- [15] C. E. Aalseth, et al., IGEX ^{76}Ge neutrinoless double beta decay experiment: Prospect for next generation experiments, *Phys. Rev. D* 65 (2002) 092007.
- [16] C. E. Aalseth, et al., The IGEX experiment reexamined: A response to the critique of Klapdor-Kleingrothaus, Dietz and Krivosheina, *Phys. Rev. D* 70 (2004) 078302.
- [17] Canberra Semiconductor NV, Lammerdries 25, B-2439 Olen, Belgium.
- [18] K.-H. Ackermann, et al., The GERDA experiment for the search of neutrinoless double beta decay in ^{76}Ge , *Eur. Phys. J. C* 73 (2013) 2330.
- [19] M. Agostini, et al., GELATIO: a general framework for modular digital analysis of high-purity Ge detector signals, *J. Instrum.* 6 (2011) P08013.
- [20] M. Agostini, et al., Off-line data processing and analysis for the GERDA experiment, *J. Phys.: Conf. Ser.* 368 (2012) 012047.
- [21] M. Agostini, et al., Measurement of the half-life of the two-neutrino double beta decay of ^{76}Ge with the GERDA experiment, *J. Phys. G* 40 (2013) 035110. arXiv:1212.3210.
- [22] M. Agostini, et al., The background in the neutrinoless double beta decay experiment GERDA, accepted by *Eur. Phys. J. C* (2013). arXiv:1306.5084, doi:10.1140/epjc/s10052-014-2764-z.
- [23] M. Agostini, et al., Pulse shape discrimination for GERDA Phase I data, *Eur. Phys. J. C* 73 (2013) 2583. arXiv:1307.2610.
- [24] for documentation see <http://tmva.sorforge.net>.
- [25] A. Caldwell, D. Kollar, K. Kröniger, BAT: The Bayesian Analysis Toolkit, *Comput. Phys. Comm.* 180 (2009) 2197.
- [26] J. Farine, EXO-200 Results, Neutrino 2012 conference, Kyoto.
- [27] M. Auger, et al., Search for Majorana neutrinos with the first two years of EXO-200 data (2014). arXiv:1402:6956.
- [28] T. R. Rodriguez, G. Martinez-Pinedo, Energy density functional study of nuclear matrix elements for neutrinoless double beta decay, *Phys. Rev. Lett.* 105 (2010) 252503.
- [29] J. Menendez, et al., Disassembling the nuclear matrix elements of the neutrinoless beta beta decay, *Nucl. Phys. A* 818 (2009) 139.
- [30] J. Barea, J. Kotila, F. Iachello, Nuclear matrix elements for double beta decay, *Phys. Rev. C* 87 (2013) 014315. arXiv:1301.4203, doi:10.1103/PhysRevC.87.014315.
- [31] J. Suhonen, O. Civitarese, Effects of orbital occupancies and spin-orbit partners on $0\nu\beta\beta$ -decay rates, *Nucl. Phys. A* 847 (2010) 207.
- [32] F. Simkovic, V. Rodin, A. Faessler, P. Vogel, Neutrinoless double beta decay and double beta decay nuclear matrix elements, quasiparticle random-phase approximation, and isospin symmetry restoration, *Phys. Rev. C* 87 (2013) 045501.
- [33] M. T. Mustonen, J. Engel, Large-Scale calculations of the double-beta decay of ^{76}Ge , ^{130}Te , ^{136}Xe , and ^{150}Nd in the deformed self-consistent Skyrme quasiparticle random-phase approximation (2013). arXiv:1301.6997.